Optical Materials 65 (2017) 15–20

Contents lists available at ScienceDirect

Optical Materials

journal homepage: www.elsevier.com/locate/optmat

First-principles calculations of electronic and optical properties of $LiCaAlF_6$ and $LiSrAlF_6$ crystals as VUV to UV solid-state laser materials

Mui Viet Luong [a, *], Melvin John F. Empizo [a], Marilou Cadatal-Raduban [b], Ren Arita [a], Yuki Minami [a], Toshihiko Shimizu [a], Nobuhiko Sarukura [a], Hiroshi Azechi [a], Minh Hong Pham [c], Hung Dai Nguyen [c], Yoshiyuki Kawazoe [d], Krista G. Steenbergen [b], Peter Schwerdtferger [b]

[a] Institute of Laser Engineering, Osaka University, 2-6 Yamadaoka, Suita, Osaka 565-0871, Japan
[b] Centre for Theoretical Chemistry and Physics, Institute of Natural and Mathematical Sciences, Massey University, Albany, Auckland 0632, New Zealand
[c] Institute of Physics, Vietnam Academy of Science and Technology, 10 Dao Tan, Ba Dinh, Hanoi, Viet Nam
[d] New Industry Creation Hatchery Center, Tohoku University, 6-6-10 Aoba, Aramaki, Aoba-ku, Sendai, Miyagi 980-8579, Japan

ARTICLE INFO

Article history:
Received 27 April 2016
Received in revised form
27 July 2016
Accepted 22 September 2016
Available online 8 October 2016

Keywords:
First-principles
Electronic band structure
Colquiriite-type fluoride crystals
Laser host materials
VUV

ABSTRACT

We report the density functional calculations of the electronic and optical properties of perfect $LiCaAlF_6$ (LiCAF) and $LiSrAlF_6$ (LiSAF) crystals. The calculations are based on the Perdew-Burke-Ernzerhof (PBE) functional employing 35% exact exchange. Using optimized unit crystal volumes and equilibrium lattice constants, both LiCAF and LiSAF are found to have indirect band gaps of 12.23 and 11.79 eV, respectively. The band gap energies of these fluoride crystals are also observed to increase upon application of pressure by uniform volume compression. Moreover, their bulk moduli are determined to be 108.01 (LiCAF) and 83.75 GPa (LiSAF), while their static dielectric constants are 1.27 (LiCAF) and 1.26 (LiSAF). Considering the dielectric functions, refractive indices, and absorption coefficients, both perfect LiCAF and LiSAF crystals are viable vacuum ultraviolet (VUV) to ultraviolet (UV) laser host media. With knowledge of the different optical transitions and pressure dependence, our results yield helpful insights on the use of these fluoride compounds as effective solid-state laser materials in the VUV region.

1. Introduction

Lithium calcium hexafluoroaluminate ($LiCaAlF_6$, LiCAF) and lithium strontium hexafluoroaluminate ($LiSrAlF_6$, LiSAF) crystals are widely used as vacuum ultraviolet (VUV) and ultraviolet (UV) laser host media [1–5]. These fluoride materials can be stimulated by the fourth harmonics of a Nd:YAG laser, i.e. 266 nm [6–8]. When doped with trivalent cerium (Ce^{3+}, Ce), the crystals become attractive UV solid-state laser hosts with a central emission wavelength of 290 nm and with a practical tuning range from 288 to 315 nm. The slope efficiencies of Ce:LiCAF and Ce:LiSAF have also been reported to reach as high as 39 and 29%, respectively. The broad gain-bandwidth of the crystals in the UV region has made them appealing for ultrashort pulse generation and amplification. Aside from being a laser material, LiCAF can be used as a lens in VUV photolithography because of its optical transmission and low thermal lensing distortion [9]. The absorption edge of LiCAF is measured to be 112 nm, while that of LiSAF is 116 nm [10,11]. Although the properties of LiCAF and LiSAF crystals have been previously studied, most reports focus on the experimental investigations thereby limiting the findings by sample quality, characterization technique, or scientific instrumentation [12–14]. Theoretical and computational investigations are necessary to supplement these experimental results to accelerate the development of compact, solid-state, and tunable laser systems. Computational simulations, such as first-principles calculations, also aid towards a better understanding of the properties of multielemental and complex materials such as these fluoride crystals. We have initially compared the electronic band structures of LiCAF and LiSAF from numerical simulations [15]. Using the ABINIT program package based on pseudopotential and plane-wave expansion methods, we initially employed local density approximation (LDA) calculations within the framework of density functional theory (DFT). We have obtained results close to some experimental values, but LDA

* Corresponding author.
E-mail address: luong-vm@ile.osaka-u.ac.jp (M.V. Luong).

http://dx.doi.org/10.1016/j.optmat.2016.09.062
0925-3467/

underestimates band gap energies as one expects from this method. On the other hand, the Perdew-Burke-Ernzerhof (PBE) functional has been used successfully in the past to investigate the electronic structure and defects of LiCAF [16]. A better approximation than LDA is needed not only for the electronic but also for the optical properties of these materials, especially when LiCAF and LiSAF will be utilized in applications through doping with Ce or other trivalent rare-earth ions such as europium (Eu^{3+}, Eu), erbium (Er^{3+}, Er), and neodymium (Nd^{3+}, Nd). We therefore perform first-principles calculations for the electronic and optical properties of perfect LiCAF and LiSAF crystals. The PBE exchange-correlation functional employing 35% exact exchange is used within the framework of DFT to calculate electronic band structures, density of states (DOS), and band gap energies. Optical properties such as dielectric functions, refractive indices, and absorption coefficients are also obtained for both fluoride crystals.

2. Crystal structure and calculation methods

LiCAF and LiSAF are colquiriite-type fluorides with a hexagonal crystal structure belonging to the P-31c space group (group number 163). Both are optically uniaxial crystals with two formula units per unit cell. Six fluorine (F) atoms surround a lithium (Li), calcium (Ca)/strontium (Sr), or aluminum (Al) atom. Each Li, Ca/Sr, and Al cation occupies a deformed octahedral site as shown in Fig. 1 (a) [17,18]. DFT calculations were completed to obtain the optimized volume, electronic band structures, total and partial DOS, and band gap energies of the LiCAF and LiSAF crystals. These calculations employed the projector-augmented wave (PAW) method as implemented within the Vienna Ab Initio Simulation Package (VASP) [19–24], with a plane-wave basis cutoff of 500 eV and the hybrid PBE density functional using 35% exact exchange [25,26]. The addition of exact exchange presents a definite improvement over the LDA description of the system properties as it improves the description of the structural, electronic, thermal, and chemical properties of wide band gap solid-state systems [27]. A previous report on LiCAF crystal implemented a hybrid functional with 38.5% exact exchange [16]. In this work, various amounts of exact exchange were initially tested, leading to the optimized value of 35% which yielded a band gap energy close to the experimental reference. The same amount of exact exchange was then used for the LiSAF crystal computations.

The perfect crystals of LiCAF and LiSAF were used with a unit cell composed of 18 atoms. The unit cell was initially optimized by using the Murnaghan equation of state to fit the curve of the total energy as a function of volume [29]. The lattice constants were then obtained from the optimized volumes to compute the band structures, DOS, complex dielectric functions, refractive indices, and absorption coefficients of the fluoride crystals. In order to generate the charge density and wave function for the first run, a $3 \times 3 \times 1$ Monkhorst-Pack k-point grid was utilized. For the band structure and DOS diagrams, the k-points were chosen following the Brillouin zone in Fig. 1 (b) with the symmetry points: Γ (0,0,0), M (1/2,0,0), K (1/3,1/3,0), A (0,0,1/2), L (1/2,0,1/2), and H (1/3,1/3,1/2) [30]. All valence band maxima of the resulting diagrams were also shifted to zero. To identify the effects of high pressure on the material properties, the pressure dependence of crystal volume and band gap energy was also investigated. Moreover, since the dielectric function is related to the electronic band structure, the complex dielectric function formed the basis of the optical property calculations such as the refractive index and absorption coefficient. The complex dielectric function, $\varepsilon(\omega)$ can be expressed as

$$\varepsilon(\omega) = \varepsilon_1(\omega) + i\varepsilon_2(\omega) \tag{1}$$

where the $\varepsilon_1(\omega)$ and $\varepsilon_2(\omega)$ are the real and imaginary parts, respectively. The imaginary part $\varepsilon_2(\omega)$ of the dielectric function is based on the Bethe-Salpeter equation and is given by Refs. [31–33]:

$$\varepsilon_2(\omega) = \left(\frac{4\pi^2 e^2}{m^2\omega^2}\right)\sum_{ij}\int \langle i|M|j\rangle^2 \left|f_i(1-f_i) \times \delta\left(E_f - E_i - \omega\right)d^3k\right. \tag{2}$$

where M is the dipole matrix, i and j are the initial and final states, respectively, f_i is the Fermi distribution for the i^{th} state, and E_i is the energy of electron in the i^{th} state. The real part $\varepsilon_1(\omega)$, on the other hand, can be calculated using the Kramers-Kronig relation

$$\varepsilon_1(\omega) = 1 + \frac{2}{\pi}P\int_0^\infty \frac{\omega'\varepsilon_2(\omega')d\omega'}{(\omega'^2 - \omega^2)} \tag{3}$$

where P is the principal value of the integral. From the components of the dielectric function, the refractive index (n) and absorption coefficient (α) can be subsequently obtained by Equations (4) and (5), respectively [34,35].

$$n(\omega) = \left[\frac{\sqrt{\varepsilon_1^2(\omega) + \varepsilon_2^2(\omega)} + \varepsilon_1(\omega)}{2}\right]^{1/2} \tag{4}$$

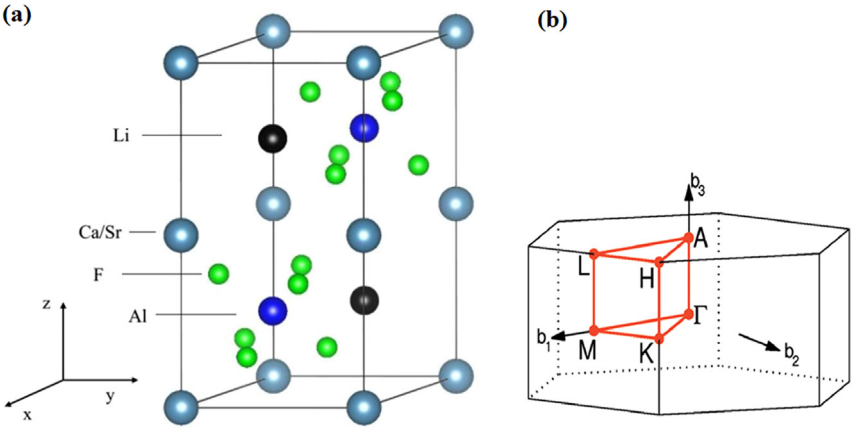

Fig. 1. (a) Colquiriite-type structure and (b) first Brilloiun zone of hexagonal unit cell of the LiCAF and LiSAF crystals.

$$\alpha(\omega) = \sqrt{2}\omega\left[\sqrt{\varepsilon_1^2(\omega) + \varepsilon_2^2(\omega)} - \varepsilon_1(\omega)\right]^{1/2} \quad (5)$$

3. Results and discussions

Fig. 2 shows the total energy as a function of the LiCAF and LiSAF crystal volumes. The total energy as a function of the unit cell volume is expressed in terms of the Murnaghan equation of state [29]. Table 1 shows the optimized crystal volumes and the *a* and *c* lattice constants of both fluoride materials. LiCAF has an optimized volume of 209.55 Å^3 with corresponding lattice constants of 4.99 (*a*) and 9.66 Å (*c*). On the other hand, LiSAF has an optimized volume of 227.71 Å^3 with corresponding lattice constants of 5.08 (*a*) and 10.25 Å (*c*). These values are larger than our previous LDA results by 0.42–5.0% and are closer to experimental values with a difference ranging only from 0.08 to 0.53%. In addition, the bulk and Young's moduli of the fluoride crystals are also obtained. LiCAF and LiSAF have calculated bulk moduli of 108.01 and 83.75 GPa, respectively. The calculated Young's moduli along the *a*- and *c*-axes are 105.32 and 94.89 GPa for LiCAF and 86.33 and 83.45 GPa for LiSAF. LiCAF's Young's moduli are close to the observed isotropic Young's modulus approximation of 96 GPa, although particular axis or direction of compression was not mentioned [38]. The Young's modulus is defined for a compression along one axis or direction, while the bulk modulus is defined for a compression where the pressure is applied uniformly along all directions. To the best of our knowledge, this is the first report regarding the Young's modulus of LiSAF and the bulk moduli of these fluoride materials.

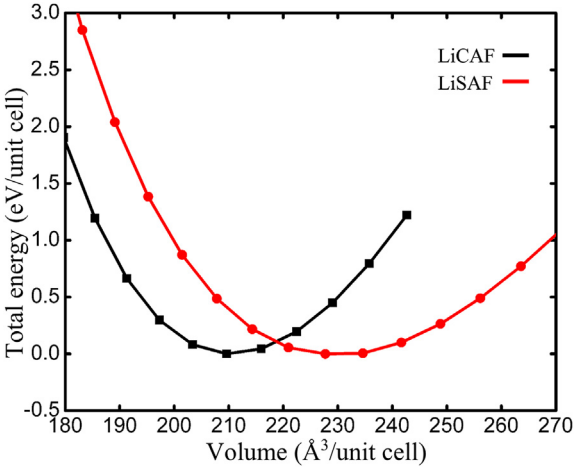

Fig. 2. Optimized volumes of the LiCAF (black) and LiSAF (red) crystals. The curves are fitted using the Murnaghan equation of state. (For interpretation of the references to colour in this figure legend, the reader is referred to the web version of this article.)

Fig. 3 illustrates the electronic band structure diagrams of LiCAF and LiSAF crystals along the high symmetry lines of the first Brillouin zone. For LiCAF, the maximum of the valence band is located at the k-point between M and K, while for LiSAF, it is located at the k-point between L and H. Similar to the conduction band minima situated at the Γ point, both materials have indirect band gaps. These band gaps have values of 12.23 and 11.79 eV for LiCAF and LiSAF, respectively. Compared with experimental results as also shown in Table 1, our present calculation gives only a difference of 3.30 or 10.51% for LiCAF and 2.99 or 10.26% for LiSAF which all indicate good agreement within an acceptable uncertainty. We have previously reported different results for the band structures of these fluoride crystals [15]. Aside from the different locations of the valence band maxima, the computed LDA band gaps for LiCAF and LiSAF were 8.02 and 7.92 eV, respectively. These values correspond to a difference ranging from 25.91 to 36.60% when compared to experimental results. Even though it gives reliable band dispersions, LDA underestimates the band gap severely in contrast to the hybrid PBE functional. We conclude that PBE + exact exchange is a better approximation of the band gap energies than LDA.

Fig. 4 shows the total and partial DOS for LiCAF and LiSAF crystals. For both fluoride compounds, the lower and upper parts of the valence band are derived from Al 3s and Al 3p and from F 2p, respectively. Similarly, the conduction band minima of the two crystals are derived from Al 3s. Ca 4s and Sr 5s also contribute to the conduction bands of LiCAF and LiSAF. When the two fluorides are compared, the Ca 3s and Ca 3p positions in the LiCAF crystal are farther from the valence band than the Sr 4s and Sr 4p positions in the LiSAF crystal. This may come from the difference in electrostatic interactions between Ca and F in LiCAF and Sr and F in LiSAF [18]. LiCAF has a smaller lattice constant than LiSAF, and the Ca–F distance is only 2.283 Å compared to 2.431 Å of Sr–F. Moreover, the Al–F (1.804 Å) electrostatic interaction is stronger than those of Li–F (2.011 Å) and Ca–F or Sr–F. The Al ion position is being distorted as the surrounding F ions are being displaced. The Sr–F interaction in LiSAF is then wider and softer than the Ca–F interaction in LiCAF with the Al distortion in these colquiirite crystals.

The fluorescence emission and absorption edge of wide band gap materials are highly dependent on the band gap energy. Band gap engineering is generally achieved through lattice distortion by changing the material composition with impurity doping. Since this method often leads to altered material properties and growth procedures, material compression under high pressure is a remarkable alternative in changing the lattice parameters while keeping the composition constant. To identify the effects of high pressure on the properties of fluoride materials, the dependence of

Table 1
Comparison of lattice constants, crystal volumes, bulk moduli, and band gap energies for the LiCAF and LiSAF crystals from previous calculations and experimental results. The values inside the parentheses indicate the percent differences from the experimental results.

Physical properties	LiCAF			LiSAF		
	Previous results (LDA) [15]	Present results (PBE)	Experimental results [28,36,37]	Previous results (LDA) [15]	Present results (PBE)	Experimental results [18,28,36,37]
Lattice constant (Å)						
a	4.97 (0.72)	4.99 (0.30)	5.01	4.99 (1.77)	5.08 (0.08)	5.08
c	9.59 (0.52)	9.66 (0.23)	9.64	10.04 (1.70)	10.25 (0.31)	10.21
Volume V_0, (Å^3)	205.76 (1.81)	208.45 (0.53)	209.55	216.82 (4.42)	227.71 (0.38)	226.84
Bulk modulus, B_0 (GPa)	–	108.01	93.4	–	83.75	–
Band gap energy, E_g (eV)	8.02 (36.60, 27.55)	12.23 (3.30, 10.51)	12.65 11.07	7.92 (34.82, 25.91)	11.79 (2.99, 10.26)	12.15 10.69

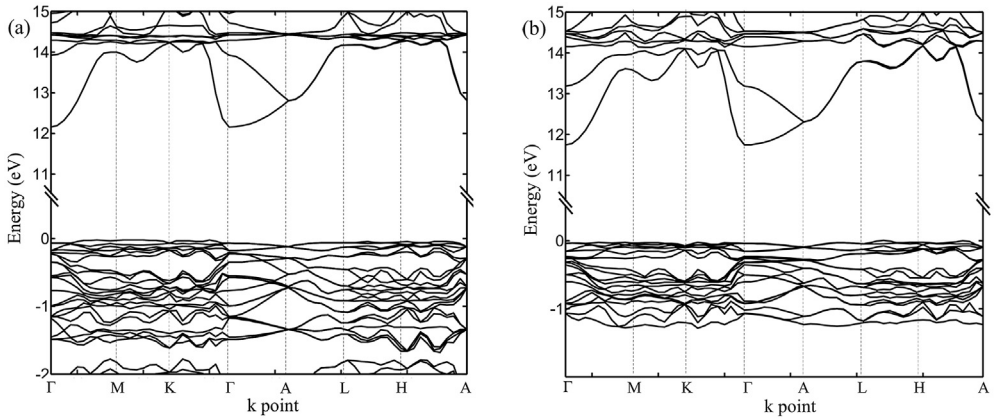

Fig. 3. Simulated electronic band structure diagrams of (a) LiCAF and (b) LiSAF crystals having indirect band gaps of 12.23 and 11.79 eV, respectively.

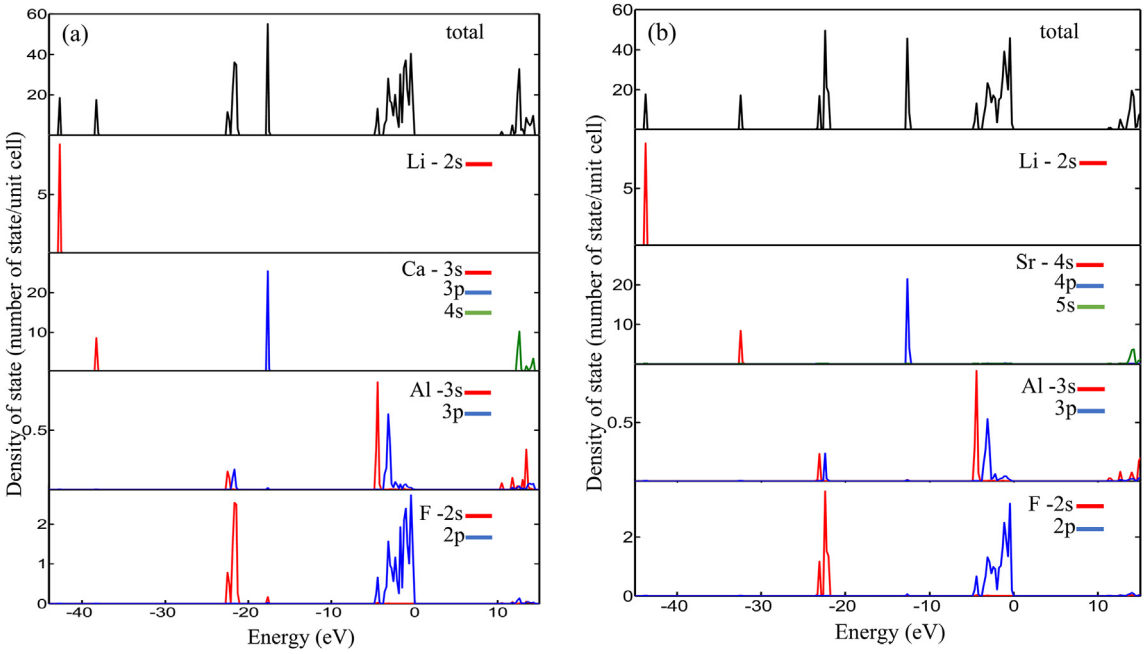

Fig. 4. Total and partial DOS of (a) LiCAF and (b) LiSAF crystals. The red, blue, and green lines represent different orbitals in each atom. With a minor contribution from Al 3s, the conduction bands of LiCAF and LiSAF are mainly derived from Ca 4s and Sr 5s, respectively. (For interpretation of the references to colour in this figure legend, the reader is referred to the web version of this article.)

the crystal volume and band gap energy on the pressure applied uniformly on the crystals is also investigated. Fig. 5 shows the crystal volume and band gap energy of the LiCAF and LiSAF crystals at different pressures. The crystal volume compression up to 10% refers to the pressure uniformly applied on the crystal in the range of 0–50 GPa. The band gap of LiCAF increases monotonically with increasing pressure. The band gap of LiSAF gradually increases but then decreases above ~36 GPa. LiSAF has a maximum band gap of 13.12 eV at 35.43 GPa. At 50.49 GPa, LiSAF has only a band gap of 13.01 eV. With a higher bulk modulus, LiCAF would behave similar to LiSAF and have a local maximum within a range higher than 50 GPa. These results imply that pure LiCAF can perform better than LiSAF in a high pressure environment. The band gap energies of the LiCAF and LiSAF crystals increase with high pressure applied through uniform volume compression. The increase of band gap energies with high pressure could be explained by the Madelung potential. When pressure is applied on the crystal, the volume is compressed, and the attractive potential of electrons and ions will increases due to the denser packing. The conduction band (LUMO) will be shifted to a higher energy while the valence band (HOMO) will be shifted to a lower energy, resulting in an increase of the band gap energy.

Our first-principles calculations of the optical properties of the LiCAF and LiSAF crystals are based on the complex dielectric function which represents the linear response of the system to an external electromagnetic field with a small wave vector. In our calculations, the excitonic effect was ignored, while the local field effect was considered. The complex shift in the Kramers-Kronig transformation is only 0.1, which is a perfectly acceptable value [39]. Fig. 6 shows the real and imaginary parts of the he complex dielectric functions of the LiCAF and LiSAF crystals. The Kramers-Kronig relation is used to extract the real part from the imaginary part of the dielectric function. An important quantity from the real part of the dielectric constant is the zero frequency limit. This value where the energy is equal to zero, i.e. $\varepsilon_1(\omega = 0)$, represents the static dielectric constant. The static dielectric constants of LiCAF and

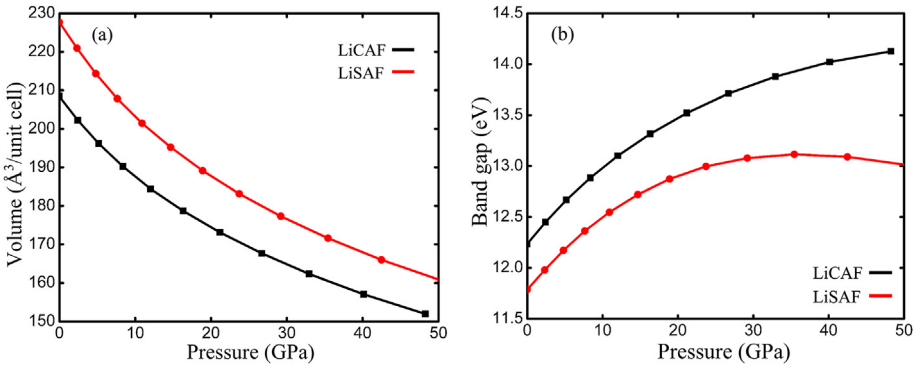

Fig. 5. Pressure dependence of (a) crystal volumes and (b) band gap energies of the LiCAF (black) and LiSAF (red) crystals. (For interpretation of the references to colour in this figure legend, the reader is referred to the web version of this article.)

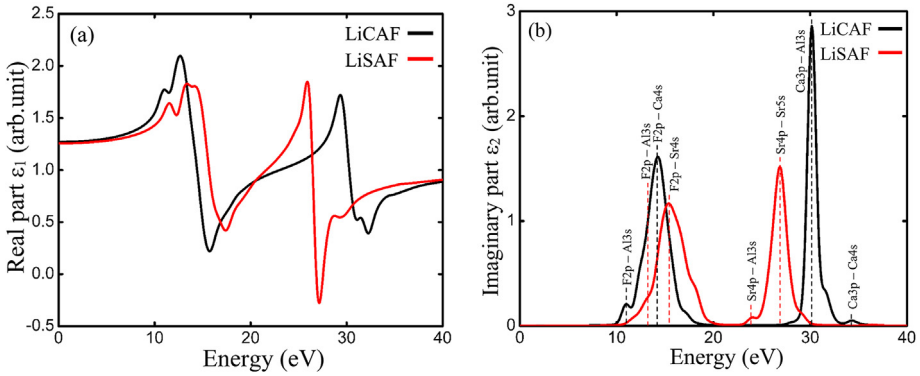

Fig. 6. (a) Real and (b) imaginary parts of complex dielectric functions of the LiCAF (black) and LiSAF (red) crystals. LiCAF and LiSAF have a static dielectric constant of 1.27 and 1.26 respectively. In addition, LiCAF and LiSAF has four peaks each in Fig. 6(b). (For interpretation of the references to colour in this figure legend, the reader is referred to the web version of this article.)

LiSAF are 1.27 and 1.26, respectively. The static dielectric constant consists of ionic and electronic contributions, and these contributions from can be calculated from the dielectric constant and the refractive index. The ionic contributions are found to be very small for LiCAF and LiSAF crystals. On the other hand, the important information from the imaginary part of the dielectric constant are the orbital transitions which can be matched to the DOS (Fig. 4). LiCAF has four peaks located at 10.97, 14.40, 30.17, and 34.28 eV which correspond to the transitions from F 2p to Al 3s, from F 2p to Ca 4s, from Ca 3p to Al 3s, and from Ca 3p to Ca 4s, respectively. In addition, LiSAF has also four peaks located at 13.09, 15.28, 24.01, and 26.97 eV which correspond to the transitions from F 2p to Al 3s, from F 2p to Sr 4s, from Sr 4p to Al 3s, and from Sr 4p to Sr 5s, respectively. Furthermore, Fig. 7 shows the refractive indices and absorption coefficients of the LiCAF and LiSAF crystals. LiCAF and LiSAF have maximum refractive indices and absorption coefficients at 13.03 and 14.55 eV, respectively. Since LiCAF and LiSAF are birefringent crystals, they have similar ordinary and extra-ordinary components of refractive indices. Our results were compared with the ordinary refractive indices for both LiCAF and LiSAF [40]. Our results differ by around 17% for LiCAF and 19% for LiSAF. For a better comparison with experimental results, the transmittance spectra of

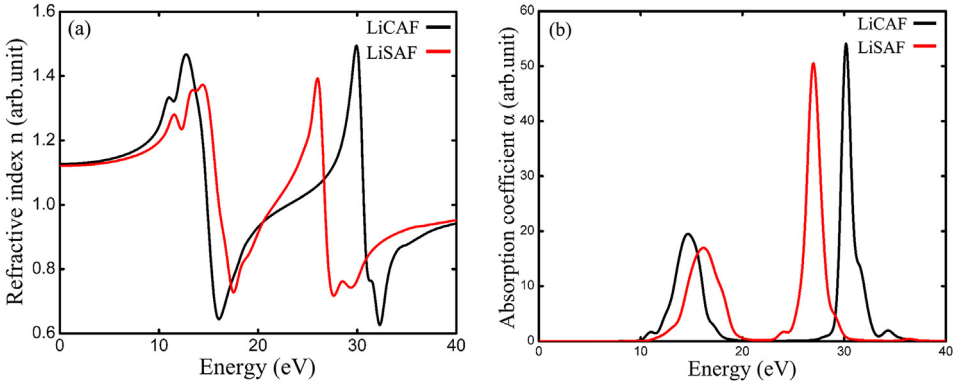

Fig. 7. (a) Refractive indices and (b) absorption coefficients of LiCAF (black) and LiSAF (red) crystals. LiCAF and LiSAF have maximum refractive indices and absorption coefficients at 13.03 and 14.55 eV, respectively. (For interpretation of the references to colour in this figure legend, the reader is referred to the web version of this article.)

LiCAF and LiSAF crystals are obtained from the calculated absorption spectra. Our transmittance spectra spanning from the VUV to the visible wavelengths are in good agreement with Ref. [8]. LiCAF and LiSAF have good transmittance down to the VUV region. In addition, previous experimental investigations report the LiCAF and LiSAF absorptions around 125 nm which was initially attributed to possible color centers or impurities [10,11]. Based on our calculations, this observed absorption can be explained by the F 2p to Al 3s transition instead of the presence of unintentional absorption centers.

With large band gaps, LiCAF and LiSAF crystals are indeed very good candidates for solid-state VUV to UV laser host media. Our first-principles calculations have identified different orbital transitions and pressure dependencies. These results will be helpful in identifying dopants or working conditions (pressure, temperature, etc.) to improve or tune the properties of the LiCAF and LiSAF crystals. Further studies on the effects of different pressures and of various dopants on the electrical and optical properties of these fluoride compounds are anticipated in near future. Experimental investigations based on the present results are expected as well.

4. Conclusion

The electronic and optical properties of perfect LiCAF and LiSAF crystals were calculated based on DFT using PBE functionals employing 35% exact exchange. Both LiCAF and LiSAF were found to have indirect band gaps of 12.23 and 11.79 eV, respectively. These results differ only by 2.99–10.51% from the experimental values. Using a better approximation than our previous LDA calculations, the dependence of the band gap energy on pressure applied by uniform volume compression was also investigated. Within a 50 GPa range, LiCAF has a maximum band gap of 14.13 eV at 48.26 GPa, while LiSAF has a maximum band gap of 13.12 eV at 35.43 GPa. Their bulk moduli are also obtained to be 108.01 (LiCAF) and 83.75 GPa (LiSAF) at zero pressure, while their static dielectric constants are 1.27 (LiCAF) and 1.26 (LiSAF). Studying the DOS and the complex dielectric functions, orbital transitions of LiCAF and LiSAF crystals were identified. Considering the optical transitions and pressure dependence, our results give helpful insights on the use of these fluoride compounds as effective laser materials in the VUV region. This leads towards the development of compact, solid-state, short-wavelength, and tunable laser systems in the future.

References

[1] J.C. Krupa, M. Queffelec, J. Alloys Compd. 250 (1997) 287–292.
[2] E. Sarantopoulou, A.C. Cefalas, in: P. Misra, M.A. Dubinskii (Eds.), VUV Laser Spectroscopy of Trivalent Rare-Earth Ions in Wide Band Gap Fluoride Crystals, Marcel Dekker, New York, 2001. Chap. 8.
[3] M. True, Y. Chen, M. Kirm, S. Vielhauer, G. Zimmerer, J. Lumin. 124 (2007) 279–285.
[4] M. True, M. Kirm, E. Negodine, S. Vielhauer, G. Zimmerer, J. Alloys Compd. 374 (2004) 36–39.
[5] M. Kirm, Y. Chen, S. Neicheva, K. Shimamura, N. Shiran, M. True, S. Vielhauer, Phys. Status Sol. C 2 (1) (2005) 418–421.
[6] C.D. Marshall, J.A. Speth, S.A. Payne, W.F. Krupke, G.J. Quarles, V. Castillo, B.H.T. Chai, J. Opt. Soc. Am. B 11 (1994) 2054–2065.
[7] J.F. Pinto, L. Esterowitz, G.J. Quarles, Electron. Lett. 31 (23) (1995) 2009–2011.
[8] K. Shimamura, S.L. Baldochi, N. Mujilatu, K. Nakano, Z. Liu, N. Sarukura, T. Fukuda, J. Cryst. Growth 211 (2000) 302–307.
[9] M. Sakai, T. Kozeki, H. Murakami, M. Hosomizu, R. Yoshioka, Y. Suzuki, S. Ono, N. Sarukura, H. Sato, T. Fukuda, in: Conference on Lasers and Electro-Optics, 2003. CTHR6.
[10] M. Sakai, Z. Liu, H. Ohtake, N. Sarukura, Y. Segawa, T. Oba, K. Shimamura, S. L. Baldochi, K. Nakano, N. Mujilatu, and T. Fukuda, CLEO'99, 497 – 498.
[11] K. Shimamura, S.L. Baldochi, I.M. Ranieri, H. Sato, T. Fujita, V.L. Mazzocchi, C.B.R. Parente, C.O. Paiva-Santos, C.V. Santilli, N. Sarukura, T. Fukuda, J. Cryst. Growth 223 (2001) 383–388.
[12] R. Arita, Y. Minami, M. Cadatal-Raduban, M.H. Pham, M.J.F. Empizo, M.V. Luong, T. Hori, M. Takabatake, K. Fukuda, K. Mori, K. Yamanoi, T. Shimizu, N. Sarukura, K. Fukuda, N. Kawaguchi, Y. Yokota, A. Yoshikawa, Opt. Mater. 47 (2015) 462–464.
[13] K. Yamanoi, T. Murata, Y. Arikawa, T. Nakazato, M. Cadatal-Raduban, T. Shimizu, N. Sarukura, M. Nakai, T. Norimatsu, H. Nishimura, H. Azechi, S. Fujino, H. Yoshida, A. Yoshikawa, N. Satoh, H. Kan, Opt. Mater. 35 (11) (2013) 1962–1964.
[14] M. Cadatal-Raduban, T. Shimizu, K. Yamanoi, K. Takeda, M.H. Pham, T. Nakazato, N. Sarukura, N. Kawaguchi, K. Fukuda, T. Suyama, T. Yanagida, Y. Yokota, A. Yoshikawa, J. Cryst. Growth 362 (2013) 167–169.
[15] M.V. Luong, M. Cadatal-Raduban, M.J.F. Empizo, R. Arita, Y. Minami, T. Shimizu, N. Sarukura, H. Azechi, M.H. Pham, H.D. Nguyen, Y. Kawazoe, Jap. J. Appl. Phys. 54 (2015) 122602.
[16] M.-H. Du, D.J. Singh, J. Appl. Phys. 112 (2012) 123516.
[17] Y. Ono, K. Nakano, K. Shimamura, T. Fukuda, T. Kajitani, J. Cryst. Growth 229 (2001) 505–509.
[18] K.I. Schaffers, D.A. Keszler, Acta. Cryst. C A7 (1991) 18–20.
[19] G. Kresse, J. Hafner, Phys. Rev. B 47 (1993) 558.
[20] G. Kresse, J. Hafner, Phys. Rev. B 49 (1994) 14251.
[21] G. Kresse, J. Furthmüller, Comput. Mat. Sci. 6 (1996) 15.
[22] G. Kresse, J. Furthmüller, Phys. Rev. B 54 (1996) 11169.
[23] P.E. Blochl, Phys. Rev. B 50 (1994) 17953.
[24] G. Kresse, D. Joubert, Phys. Rev. B 59 (1999) 1758.
[25] J.P. Perdew, K. Burke, M. Ernzerhof, Phys. Rev. Lett. 77 (1996) 3865.
[26] J.P. Perdew, K. Burke, M. Ernzerhof, Phys. Rev. Lett. 78 (1997) 1396.
[27] J.P. Perdew, M. Ernzerhof, K. Burke, J. Chem. Phys. 105 (1996) 9982–9985.
[28] K. Shimamura, H. Sato, A. Bensalah, H. Machida, N. Sarukura, T. Fukuda, J. Alloys Compd. 343 (2002) 204–210.
[29] V.G. Tyuterev, N. Vast, Comput. Mater. Sci. 38 (2006) 350–353.
[30] W. Setyawan, S. Curtarolo, Comput. Mater. Sci. 49 (2010) 299–312.
[31] F. Bassani, G. Pastroi, Parravicini, Electronic States and Optical Transitions in Solids, Pergamon Press, Oxford, 1973.
[32] P. Puschnig, C. Ambrosch-Draxl, Phys. Rev. B 66 (2002) 165105.
[33] S. Sharma, C. Ambrosch-Draxl, M.A. Khan, P. Blaha, S. Auluck, Phys. Rev. B 60 (1999) 8610.
[34] M. Fox, Optical Properties of Solids, Oxford University Press, New York (, 2001.
[35] M. Dreesel, G. Gruner, Electrodynamics of Solid: Optical Properties of Electron in Matter, Cambridge University Press, UK, 2002.
[36] N. Shiran, A. Gektin, S. Neicheva, M. Weber, S. Derenzo, M. Kirm, M. Truec, I. Shpinkov, D. Spassky, K. Shimamura, N. Ichinose, Nucl. Instrum. Methods Phys. Res. Sect. A 537 (2005) 266–270.
[37] A. Bensalah, K. Shimamura, K. Nakano, T. Fujita, T. Fukuda, J. Cryst. Growth 231 (2001) 143–147.
[38] B.W. Woods, S.A. Payne, J.E. Marion, R.S. Hughes, L.E. Davis, J. Opt. Soc. Am. B 8 (5) (1991) 970–977.
[39] F. Wooten, Optical Properties of Solids, Academic Press, New York, 1972.
[40] R.D. Peterson, A.T. Pham, H.P. Jenssen, A. Cassanho, V. Castillo, in: M. Fejer, H. Injeyan, U. Keller (Eds.), Advanced Solid State Lasers, Vol. 26 of OSA Trends in Optics and Photonics (Optical Society of America), 1999 paper TuB6.